NANO LETTERS

pubs.acs.org/NanoLett

Letter

Electrically Driven Hyperbolic Nanophotonic Resonators as High Speed, Spectrally Selective Thermal Radiators

John Andris Roberts, Po-Hsun Ho, Shang-Jie Yu, and Jonathan A. Fan*

Cite This: *Nano Lett.* 2022, 22, 5832−5840

Read Online

ACCESS | Metrics & More | Article Recommendations | Supporting Information

ABSTRACT: We introduce and experimentally demonstrate electrically driven, spectrally selective thermal emitters based on globally aligned carbon nanotube metamaterials. The self-assembled metamaterial supports a high degree of nanotube ordering, enabling nanoscale ribbons patterned in the metamaterial to function both as Joule-heated incandescent filaments and as infrared hyperbolic resonators imparting spectral selectivity to the thermal radiation. Devices batch-fabricated on a single chip emit polarized thermal radiation with peak wavelengths dictated by their hyperbolic resonances, and their nanoscale heated dimensions yield modulation rates as high as 1 MHz. As a proof of concept, we show that two sets of thermal emitters on the same chip, operating with different peak wavelengths and modulation rates, can be used to sense carbon dioxide with one detector. We anticipate that the combination of batch fabrication, modulation bandwidth, and spectral tuning with chip-based nanotube thermal emitters will enable new modalities in multiplexed infrared sources.

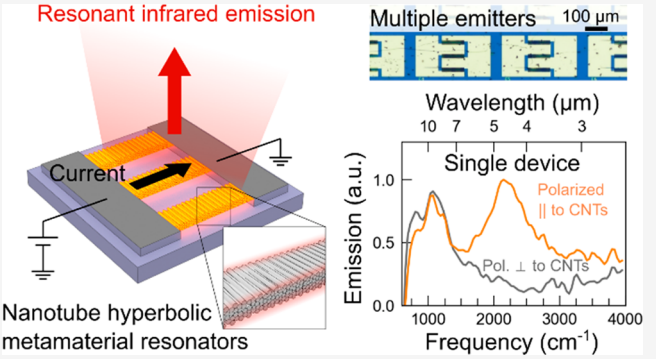

KEYWORDS: *infrared, nanophotonics, thermal emission, hyperbolic materials, carbon nanotubes*

Mid-infrared light sources are the basis for numerous applications in environmental monitoring, industrial safety, and security.[1] An ideal light source would combine low cost, a narrowband emission spectrum that coincides with a desired molecular resonance frequency, and a high modulation rate that enables frequency-multiplexed detection schemes. Advanced optoelectronic sources based on quantum cascade lasers and mid-infrared light emitting diodes offer fast modulation speeds, but their high cost precludes their use in many mainstream applications.[2] As such, the most common infrared sources in conventional systems are incandescent emitters that utilize an electrically heated filament for thermal emission.[3,4] Traditional incandescent sources are cheap to fabricate and package, but they emit light across a broad wavelength range and have modulation rates limited to approximately 10 Hz,[5] making them less than ideal in many applications.

These fundamental limitations have motivated the development of thermal emitters with new capabilities.[6−8] In most cases to date, approaches have been proposed that enhance either spectral selectivity or modulation rate. Spectrally tailored thermal emitters have been made possible by globally heating metamaterials,[9−21] which are subwavelength-scale structured media that can support narrowly peaked emissivity spectra corresponding to engineered absorptive resonances, as dictated by Kirchhoff's law. Fast modulation from thermal emitters has been achieved by use of innovative materials that feature novel tuning mechanisms[22−26] or exceptionally small volumes,[27−32] which enable fast variations in temperature[33−35] though with limited spectral control. Hybrid device schemes that couple thermal emitters to optical cavities can combine fast modulation with spectral selectivity,[27,29,34−36] but their implementation in the form of multiple fast emitters operating at unique wavelengths remains an integration challenge.

Material platforms that can be readily patterned into optically resonant devices with low thermal mass offer an alternative and scalable route to constructing high speed, spectrally selective thermal emitters. Globally aligned carbon nanotube (CNT) films[37−39] that feature emergent bulk optoelectronic properties, such as hyperbolic dispersion,[40−45] present new opportunities in this domain. CNTs are a maturing materials system for electronic and photonic applications, and they are an established material for electrically driven incandescence,[36,46−52] with temperature stability up to 1600 °C under vacuum.[53] As hyperbolic media, in which the optical dielectric function possesses values with opposite signs along different axes, they enable the implementation of low thermal mass infrared hyperbolic

Received: April 20, 2022
Revised: July 7, 2022
Published: July 18, 2022

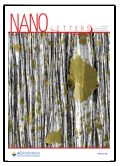

https://doi.org/10.1021/acs.nanolett.2c01579
Nano Lett. 2022, 22, 5832−5840

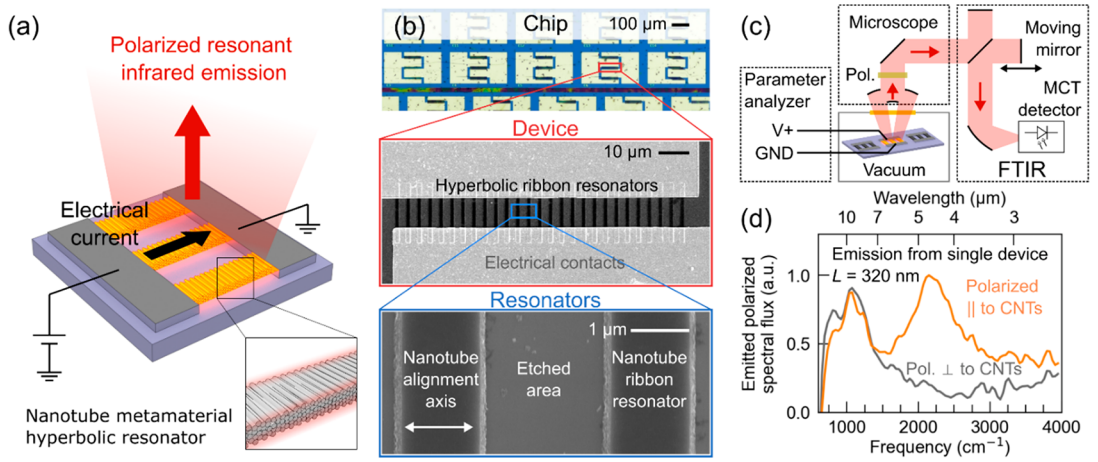

Figure 1. Device configuration and emission spectra of CNT metamaterial nanoribbons. (a) Device concept showing carbon nanotube (CNT) metamaterial ribbons functioning as both resistive heaters and hyperbolic mid-infrared resonators. (b) Top: Optical microscope image of a chip with several devices fabricated from a single globally aligned CNT film on a thermally oxidized silicon substrate. Middle: Scanning electron micrograph (SEM) of a row of resonators in one device. Bottom: High magnification SEM of two resonators (darker areas), with the alignment direction of the CNTs indicated. (c) Schematic of the measurement apparatus. The sample is mounted in a high-vacuum chamber with a window, and a single device is electrically probed. Thermal emission from the single device is collected by a microscope objective, and its spectrum is measured using an FTIR spectrometer. A polarizer can be rotated to analyze the polarization of emitted light. (d) Emission spectra from a single device with L = 320 nm driven with 14 mA of current, polarized along (orange) and perpendicular to (gray) the CNT alignment axis. A polarized emission peak at wavelengths near 4.5 μm corresponds to thermal emission mediated by the hyperbolic plasmon mode. The spectra are normalized using the measured relative instrument response function so that the result is a spectral flux in arbitrary units (see Supporting Information).

resonators that can scale down to dimensions of hundreds of nanometers.[54,55] In prior studies, the characterization of such nanostructures at room temperature[40−44] and their measured thermal emission characteristics upon global heating[45] confirmed the presence of these hyperbolic properties across a wide temperature range.

We propose and demonstrate thermal emitters based on CNT hyperbolic metamaterials that function as both high-speed electrically driven heaters and optically resonant, spectrally selective nanostructures. A schematic of our device implementing this concept is shown in Figure 1a. A CNT metamaterial is prepared in bulk using vacuum filtration and patterned into nanoribbons that function as infrared hyperbolic metamaterial resonators capable of confining light to extreme, subwavelength-scale dimensions.[40,41] At the hyperbolic resonance frequency, the nanoribbon array has increased absorption, which translates to increased narrowband emissivity and subsequent spectrally selective thermal emission upon heating. The nanoribbons are resistively heated by direct electrical biasing so that the CNT nanoribbons function as both optical hyperbolic resonators and heating elements with a small heated volume and short thermal time constant.

The key advance represented by this work is that because the CNT incandescent filaments are inherently spectrally selective without the use of an external resonator, multiple electrically driven thermal emitters, designed for different wavelengths and with fast modulation rates, can be fabricated side-by-side on one chip. The implementation of this concept is enabled by the large area, temperature stability, and anisotropy of the nanotube hyperbolic metamaterial. In contrast to prior demonstrations of electrically driven emitters based on individual and disordered ensembles of CNTs, our CNT metamaterials can be patterned into deep-subwavelength-scale resonators at a wavelength that is tunable through the resonator geometry.[40,44,45] Other infrared hyperbolic materials,[55−57] such as layered semiconductors, graphene structures, or phonon-polaritonic materials, cannot simultaneously provide the large areas, stability at high temperatures, wavelength tunability, and resistive heating that are required for use as both a hyperbolic resonator and an incandescent filament.

The fabricated devices on a silicon substrate are shown in Figure 1b. As shown in the top optical microscope image, many emitters can be patterned on one chip because the vacuum filtration process creates chip-scale CNT films with global alignment and consistent thickness. Each emitter can be designed to emit at a different resonant wavelength by varying the ribbon width, L, and angle relative to the CNT alignment axis, θ, which alters the Fabry−Pérot resonance condition of the hyperbolic waveguide modes in the ribbon.[40] Each device comprises three arrays of CNT ribbons with the same values of L and θ, which are connected in parallel using interdigitated metal electrodes. The interdigitated structure allows for relatively short ribbon lengths (10 μm), which reduces the likelihood of a given ribbon having a defect that severs its electrical conductivity while maintaining a large enough total emitting area. Values of L range between 320 and 900 nm, and the CNT film has a thickness of ∼115 nm (see Supporting Information).

We measure the infrared spectrum of emitted light from individual devices using a Fourier transform infrared (FTIR) spectrometer coupled to a microscope,[60−62] depicted in Figure 1c. The device is kept under high vacuum to prevent burning while a bias is applied using a semiconductor parameter analyzer (see the Supporting Information for details). A polarizer is used while measuring light emitted from the device because the CNT hyperbolic plasmon resonance is known to couple to light polarized along the CNT alignment axis,[58,59,40] and we expect the resonant thermal emission to be polarized along this axis. We perform automated, cycled emission measurements to obtain emission spectra for both polarizations (see Supporting Information).

https://doi.org/10.1021/acs.nanolett.2c01579
Nano Lett. 2022, 22, 5832−5840

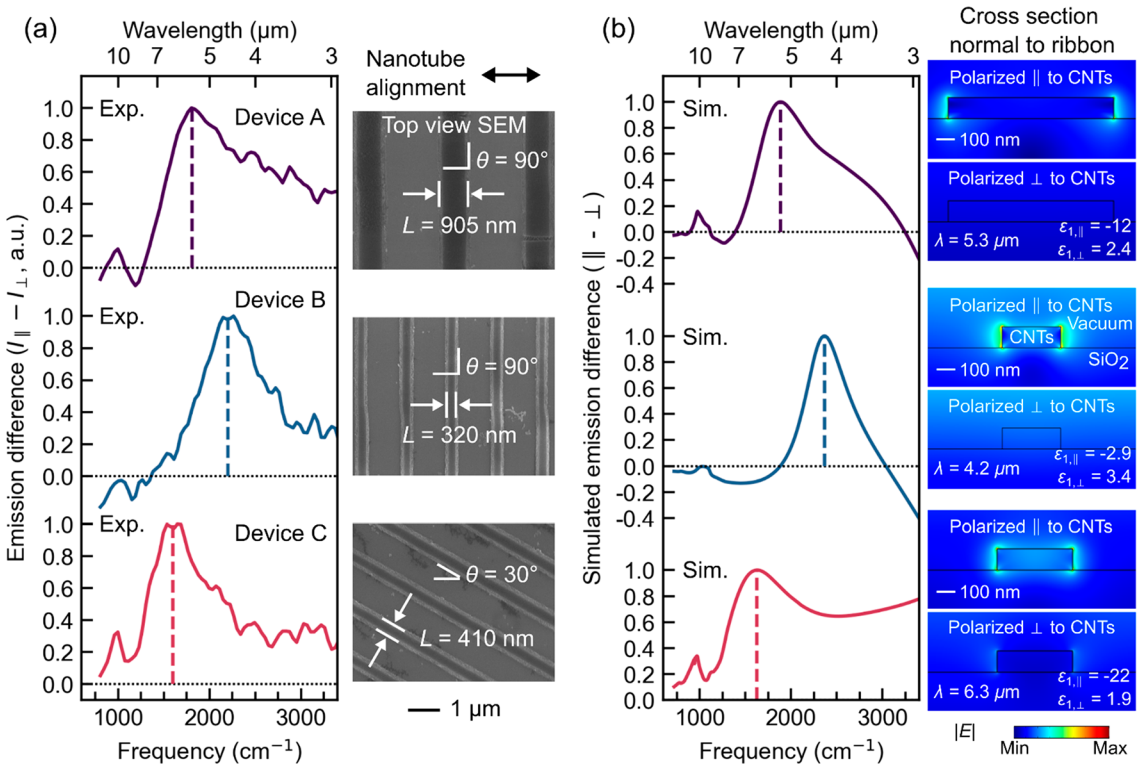

Figure 2. Hyperbolic thermal radiators emitting at different peak wavelengths. (a) Polarization-difference emission spectra $I_{\parallel}(\omega) - I_{\perp}(\omega)$ of three devices patterned in the same CNT film with varying ribbon geometric parameters. Top: Device A, with relatively wide ribbons (L = 905 nm) in a normal-cut direction (θ = 90°), measured at 30 mA. Middle: Device B, with relatively narrow ribbons (L = 320 nm) in a normal-cut direction (θ = 90°), at 14 mA (the same data as in Figure 1c). Bottom: Device C, with relatively narrow ribbons (L = 410 nm) in an off-axis direction (θ = 30°), at 17.5 mA. Ribbons featuring wider widths and off-normal cut angles show red-shifted resonances. (b) Modeled emission spectra corresponding to each device, with ribbon cross-section electric field profiles from finite element optical simulations showing the hyperbolic resonance.

The measured emission spectra from these devices show clear emission peaks originating from the hyperbolic resonances of the metamaterial nanoribbons. Figure 1d shows the emission spectra for each polarization from a representative device with L = 320 nm and θ = 90° under a constant 14 mA bias. Two main spectral features are apparent. Near 4.5 μm, an emission peak appears that is polarized along the CNT alignment axis. This polarization signature is expected for the hyperbolic plasmon resonance, and the peak appears at a frequency near where the CNT metamaterials were previously observed to have hyperbolic dispersion.[40,41] An unpolarized emission peak at wavelengths near 10 μm can be attributed to a phonon resonance in the SiO_2 substrate[63] and indicates substrate heating.

To further probe the origin of the thermal emission resonance and its tunability, we repeat these emission measurements using devices with different ribbon widths and angles, all patterned from the same CNT film on one chip. The scaling trends we observe indicate that the polarized emission peak arises from the hyperbolic plasmon resonance in the nanotube metamaterial ribbons and demonstrate that multiple emitters with different peak wavelengths can be patterned in one step on the same device. Figure 2a shows the emission spectra of three devices, with the device from Figure 1c shown as device B. We plot the difference in emitted spectral flux between polarizations parallel and perpendicular to the CNT axis, $I_{\parallel}-I_{\perp}$, because the resonance of interest is polarized along the CNT alignment axis. Device A has wider ribbon resonators (L = 905 nm) than device B, with a ribbon direction that is still perpendicular to the CNT alignment axis (θ = 90°). In the hyperbolic resonator model, we expect the resonance to be at a lower frequency for wider ribbons, as previously observed in far-field transmission measurements.[40,58] As expected, the resonance appears at a longer wavelength, with a peak near 5.5 μm. The nanoribbons in device C are slightly wider than those in device A, with L = 410 nm, but feature a CNT alignment angle of θ = 30°. Peak thermal emission in these devices shifts to even longer wavelengths, with a maximum near 6.5 μm, because the resonant hyperbolic waveguide mode in the nanoribbon lies along a portion of the hyperbolic isofrequency surface featuring a large in-plane wavevector.[40] While we report a limited number of emitters following these trends in this work, we have previously observed them in dozens of passive resonator arrays studied with transmission spectroscopy that gave results in agreement with electromagnetic modeling.[40,44]

A theoretical model of the emission spectra agrees well with our experimental findings and further reinforces that the hyperbolic metamaterial resonances control the emission spectra. We use the local Kirchhoff law for an anisothermal emitter because the CNT resonators are locally heated,[35,64] and we consider a simplistic model that assumes that the emission originates from CNT resonators at one temperature, T_{CNT}, and from the heated oxide at an arbitrarily assumed temperature T_{ox}. We model the integrated absorption of each component using a two-dimensional finite element method electromagnetic simulation (see the Supporting Information) with previously measured effective dielectric functions for the CNT metamaterial.[40,41] Our model gives emission spectra that agree well with the experimentally measured spectra (Figure

https://doi.org/10.1021/acs.nanolett.2c01579
Nano Lett. 2022, 22, 5832−5840

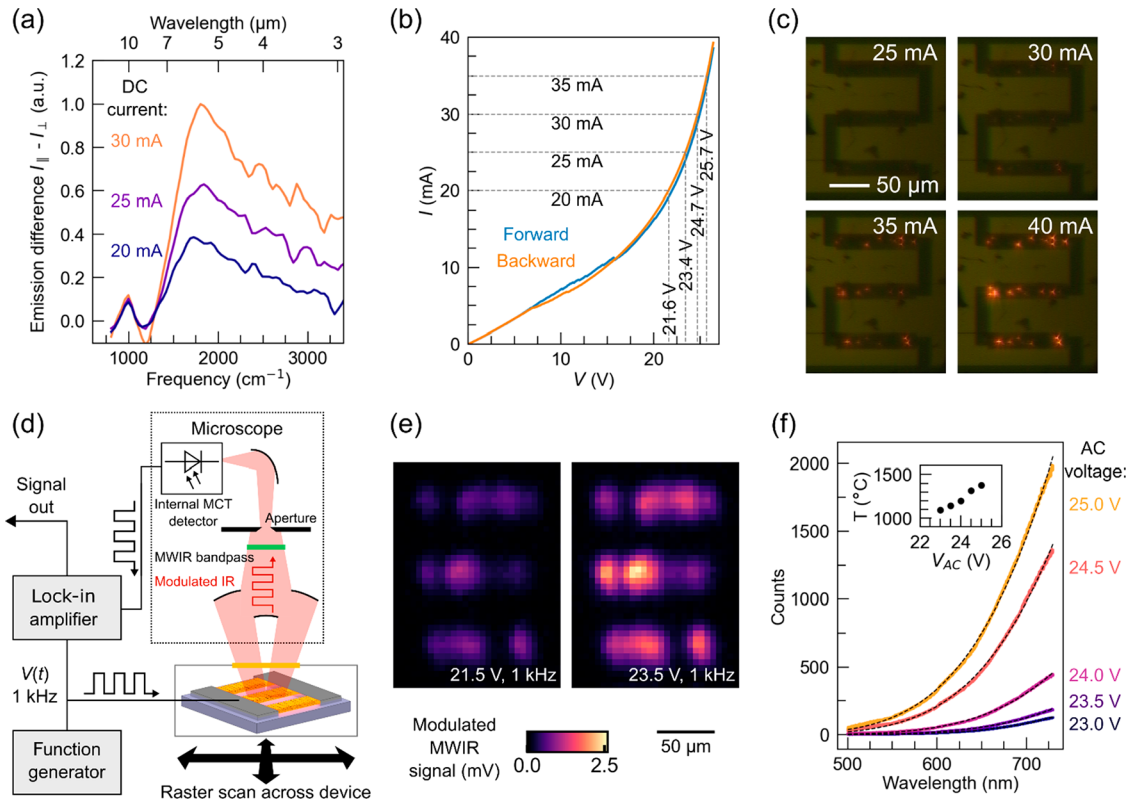

Figure 3. Characterization of the emission from a device. (a) Polarization-difference emission spectra from device A at several values of the DC current bias. (b) Measurement of the current as a function of bias voltage for device A with values corresponding to different measurement conditions marked. (c) Optical microscope images of device A under DC bias at several current levels showing the appearance of visible hot spots and nonuniformity. (d) Schematic of the apparatus used to map the mid-wave infrared emission intensity across the device using a single-element detector in the microscope. The aperture limits the field of view to a small spot. The device bias is modulated with a square wave, and the mid-wave infrared (MWIR, 3−5 μm) light received by the microscope's single-element detector is measured using a lock-in amplifier. The stage is mechanically scanned to measure the signal at points across the device to form an image. (e) Maps of the MWIR emission intensity from device A, showing that MWIR emission appears to be correlated with visible hot spots. (f) Visible emission spectra of device A with fits to Planck's law. Inset: Best-fit values of the temperature for each bias condition.

2b). The polarized emission peak originates from a resonance in the CNTs with a spectral shape and simulated field profiles (Figure 2b, right) consistent with earlier modeling of the CNT hyperbolic resonance.[40,44] The agreement between this model and the experimentally observed emission spectra confirms our hyperbolic model of the resonance and highlights the stability of the hyperbolic resonance at high temperatures.

Since the emission spectrum is controlled by the resonance, we expect its shape and peak frequency to be relatively insensitive to the temperature of the resonators. We find experimentally that the peak emission frequency is stable while the ribbon resonators go through large changes in the bias current. Figure 3a shows the emission spectra of device A at several values of the bias current, showing that the resonant emission frequency is relatively constant as a function of current. The $I-V$ curve of device A (Figure 3b) shows that the current increases rapidly across the range of voltages where we measure the infrared spectrum, corresponding to a significant increase in Joule heating across this range.

To probe the heating dynamics within the device, we image the emitted light at multiple wavelengths. Visible images of the devices, when driven with larger currents, show nonuniform emission with apparent hot spots (Figure 3c). To investigate the role of hot spots in the resonant infrared emission process, we constructed the apparatus shown in Figure 3d to map the infrared emission intensity across a device. Images of the mid-wave infrared emission from device A (Figure 3e) confirm that it originates from hot spots. Additionally, the locations of the infrared hot spots at lower biases are visually correlated with the locations of the visible hot spots at higher biases. Although hot spots dominate the thermal emission process, the agreement in Figure 2 between the experimental and modeled emission spectra, assuming one temperature, indicates that the peak emission wavelength is dictated by the hyperbolic resonance and the range of temperatures present in the device does not significantly broaden the resonant emission.

We estimate the peak temperatures of the devices by measuring their visible emission spectra. The visible emission spectra of device A at several square-wave bias levels are shown in Figure 3f. In the visible wavelength range, we expect the CNT metamaterial to have a relatively uniform emissivity spectrum[41] so that we can estimate a temperature by fitting Planck's law to the emission spectrum. The resulting temperatures are shown in the inset of Figure 3f and range roughly from 1090 °C to 1380 °C for biases comparable to those applied during the infrared spectroscopy measurements. Although precise interpretation of this temperature is difficult due to the nonuniformity of the emission, it represents a characteristic temperature for the parts of the device that dominate emission.

A key feature of the incandescent-resonator device design is that the heated volume is small and in direct contact with the

https://doi.org/10.1021/acs.nanolett.2c01579
Nano Lett. 2022, 22, 5832−5840

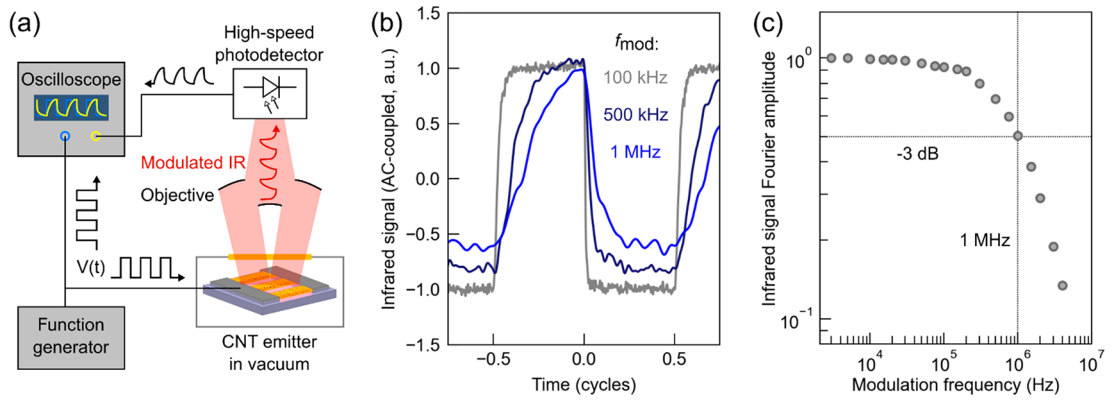

Figure 4. Modulation of the thermal radiation up to 1 MHz. (a) Schematic of the modulation measurement setup. An external objective is used to couple light emitted from the device (under vacuum) to a high-speed HgCdTe photodetector with a 10.6 μm cutoff wavelength. The device is driven using a square wave, and the drive voltage and detector signal are recorded using an oscilloscope. (b) Signal collected from device A biased using a square wave (3−23 V) at 100 kHz, 500 kHz, and 1 MHz. The signals are digitally low-pass-filtered to remove noise. See the Supporting Information for details. (c) Normalized Fourier amplitude of the signal from device A as a function of the modulation frequency, showing modulation of the thermal radiation at rates up to 1 MHz.

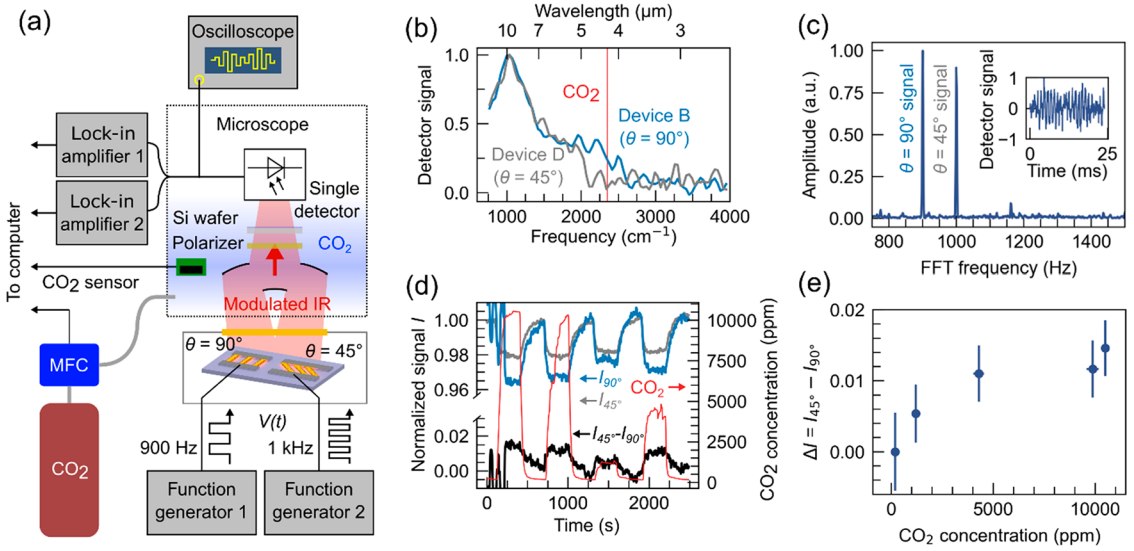

Figure 5. Gas sensing with a single detector, using multiple emitters at different emission wavelengths and modulation frequencies. (a) Schematic of the sensing concept. Two devices with different ribbon parameters are simultaneously biased at two different modulation frequencies, and light is collected with one detector. CO_2 concentration along the optical path is controlled using a mass flow controller. (b) Measured emission spectra of the two devices at relatively low biases (10 mA for device B, 8 mA for device D) for polarization along the CNT axis. Device B has more emission at the CO_2 absorption frequency than device D, where the hyperbolic resonance is red-shifted due to the 45° ribbon angle. The spectra are not corrected for the instrument response since the raw detector signal is measured. (c) Total signal from the HgCdTe detector (inset) recorded by the oscilloscope showing a beat pattern, with the Fourier transformed spectrum showing one peak from each device (see the Supporting Information for measurement details). (d) Amplitudes of the signal from each device (blue and gray) and their difference (black), measured using the lock-in amplifiers and normalized to the levels with no CO_2, as the CO_2 concentration varies. Device B (θ = 90°) shows larger attenuation with increasing CO_2 concentration. (e) Difference between the signals from devices D (θ = 45°) and B (θ = 90°) at different CO_2 concentrations based on the data in (d). The difference increases with CO_2 concentration. Error bars correspond to the variation in values within the range of times when the CO_2 level is considered stable (200−300 s after each flow rate change).

substrate, leading to a short thermal time constant and the potential for modulation much faster than is possible with traditional incandescent emitters. We use a high-speed mid-infrared detector to quantify the response time of our CNT metamaterial emitter (Figure 4a). When operated with a square-wave pulsed drive voltage, the amplitude of the emitted thermal radiation from device A shows asymmetric rise and fall times on the order of hundreds of nanoseconds (Figure 4b). The maximum modulation rate is ∼1 MHz measured by the −3 dB frequency of the Fourier component of the infrared emission at the drive voltage (Figure 4c).

This modulation rate corresponds to time constants of the order expected for thermal diffusion in the CNT film. This characteristic time scale[35] is given by t^2/D, where t is the CNT film thickness and $D = k/(\rho C_p)$ is the thermal diffusivity with thermal conductivity k and volumetric heat capacity ρC_p. Using the film thickness t = 115 nm and a value of k = 0.085 W m^{-1} K^{-1} recently reported for a similar CNT film in the perpendicular direction,[65] with a density[66] ρ = 1.3 g cm^{-3} and the heat capacity of graphite[67] at 1000 °C, gives a thermal diffusion time constant ∼400 ns, similar to the experimental result. Higher-fidelity thermal modeling is not feasible given

https://doi.org/10.1021/acs.nanolett.2c01579
Nano Lett. 2022, 22, 5832−5840

the unknown hot spot sizes and thermal parameters. While these time scales are much longer than for nanoscale metallic films because of the low thermal conductivity of the CNTs in the perpendicular direction, they are orders of magnitude faster than the incandescent sources typically used in commercial infrared sensors.

The megahertz modulation bandwidth, together with the ability to batch-fabricate emitters, may enable advances in sensing systems such as high-speed measurements and multichannel sensing multiplexed by modulation frequency. As a proof-of-concept demonstration, we show how two CNT emitters on a single chip, emitting at different wavelengths and with different modulation frequencies, can be used as compact and integrated radiation sources for gas sensing. Our emitter platform is conceptually different from typical nondispersive infrared (NDIR) gas sensors, which use one broadband thermal emitter[3,5] and a pair of detectors with spectral filters tuned to either the gas absorption line or a reference wavelength. Recent work has used spectrally selective metamaterials to replace the broadband emitter or detector[68−71] but has not incorporated fast modulation or modulation frequency multiplexing. Our emitter concept enables a different system design where multiple spectrally selective emitters, at the gas absorption wavelength and with a detuning, can be received simultaneously by a single broadband detector and distinguished using modulation-frequency multiplexing. In general, more emitters on one chip could be operated simultaneously for spectroscopic sensing of broad spectral ranges or detection of multiple gases.

We implement this concept using two CNT emitters on one chip and demonstrate the basic capability to sense CO_2 gas. Figure 5a shows a detailed schematic of the measurement. Device B, which has a hyperbolic resonance overlapping the CO_2 absorption line[3] at 2349 cm^{-1} (Figure 5b), is biased with a square wave at 900 Hz while an adjacent device (device D), having the same patterned ribbon width but at an angle θ = 45° to redshift the hyperbolic resonance away from the CO_2 absorption frequency (Figure 5b), is simultaneously biased at 1 kHz for use as a reference. As the CO_2 concentration increases, we expect the signal from device B (θ = 90°) to be attenuated more strongly than that from device D (θ = 45°). The light emitted from both devices is received by a single-element broadband detector. A portion of the overall signal from the single-element detector is shown in the inset of Figure 5c and displays a beat pattern resulting from the two device signals at slightly different frequencies. The Fourier transform of the detector signal shows peaks at the modulation frequencies for each device (Figure 5c).

The amplitudes of these channels (900 Hz sensing and 1 kHz reference) are shown in Figure 5d as the CO_2 concentration inside the microscope is varied. Both channels show a decrease in amplitude at higher CO_2 concentration (Figure 5d). As expected, device B (θ = 90°) is attenuated more strongly, and the difference in attenuation between devices B and D increases with CO_2 concentration (Figure 5e), indicating the potential to use the pair of devices as a sensor. To implement a higher-performance sensor, it will be necessary to improve the stability and output power of the emitters and to use the full inch-scale CNT films, from which emitter size can be scaled significantly beyond the microscopic footprints of the devices used in this work (330 μm × 180 μm, including contact pads).

In summary, we demonstrate that electrically driven CNT metamaterial ribbons emit spectrally selective thermal radiation at a wavelength determined by the CNT hyperbolic resonance, which can be tuned through the design of the ribbon pattern. All seven devices we measured with this design (the four discussed here and three others; see Supporting Information) showed the polarized emission peak associated with the hyperbolic resonance. Thus, despite the presence of material defects featured in each device, it was already possible to reliably fabricate emitters operating at a prespecified wavelength. Future work will be needed to understand and mitigate the occurrence of nonuniformity to improve device stability and output power. This may involve further optimization of the vacuum filtration and CNT film transfer processes.[72] Varying the film preparation parameters will also allow trade-offs between efficient heating of a thick, thermally insulating CNT film and fast modulation in thin films, as well as tuning of the film's hyperbolic properties through the CNT composition. These design degrees of freedom will complement the tunability of the hyperbolic resonance through the ribbon geometry. We anticipate that the ability to easily integrate emitters tuned to different wavelengths on one chip, with megahertz modulation rates, will enable new system concepts in infrared sensing and communication. Recent demonstrations of infrared hyperbolic behavior in a number of van der Waals materials[73−76] suggest the possibility of extending this device concept to the ultimate low-thermal-mass limit of a two-dimensional resonator, if material candidates with large areas and high temperature stability can be realized.

■ ASSOCIATED CONTENT

Supporting Information

The Supporting Information is available free of charge at https://pubs.acs.org/doi/10.1021/acs.nanolett.2c01579.

Details of device preparation and characterization, initial biasing and device stability, details of infrared and visible measurements, spectra of additional devices, and model for thermal emission spectra (PDF)

■ AUTHOR INFORMATION

Corresponding Author

Jonathan A. Fan − *Department of Electrical Engineering, Stanford University, Stanford, California 94305, United States;* orcid.org/0000-0001-9816-9979; Phone: (650) 723-0278; Email: jonfan@stanford.edu

Authors

John Andris Roberts − *Department of Applied Physics, Stanford University, Stanford, California 94305, United States;* orcid.org/0000-0002-9995-5346

Po-Hsun Ho − *Department of Electrical Engineering, Stanford University, Stanford, California 94305, United States*

Shang-Jie Yu − *Department of Electrical Engineering, Stanford University, Stanford, California 94305, United States;* orcid.org/0000-0002-5507-8425

Complete contact information is available at: https://pubs.acs.org/10.1021/acs.nanolett.2c01579

Author Contributions

J.A.R. and J.A.F. conceived the experiment. P.-H.H. performed the vacuum filtration process. S.-J.Y. configured the vacuum

https://doi.org/10.1021/acs.nanolett.2c01579
Nano Lett. 2022, 22, 5832−5840

stage and performed AFM measurements. J.A.R. performed nanofabrication, optical and electrical measurements, analysis, and simulations. All authors wrote and edited the manuscript.

Notes

The authors declare no competing financial interest.

■ ACKNOWLEDGMENTS

This work was supported by the Air Force Office of Scientific Research (AFOSR) Multidisciplinary University Research Initiative (MURI) under Award FA9550-16-1-0031 and by the National Science Foundation under Award 2103721. J.A.R. was supported by the Department of Defense through the National Defense Science and Engineering Graduate Fellowship Program. Part of this work was performed at the Stanford Nano Shared Facilities (SNSF) and the Stanford Nanofabrication Facility (SNF), supported by the National Science Foundation under Award ECCS-2026822.

■ ABBREVIATIONS

CNT, carbon nanotube; FTIR, Fourier transform infrared; MWIR, mid-wave infrared; NDIR, nondispersive infrared

■ REFERENCES

(1) Potyrailo, R. A. Multivariable Sensors for Ubiquitous Monitoring of Gases in the Era of Internet of Things and Industrial Internet. *Chem. Rev.* **2016**, *116* (19), 11877−11923.
(2) Krier, A.; Repiso, E.; Al-Saymari, F.; Carrington, P. J.; Marshall, A. R. J.; Qi, L.; Krier, S. E.; Lulla, K. J.; Steer, M.; MacGregor, C.; Broderick, C. A.; Arkani, R.; O'Reilly, E.; Sorel, M.; Molina, S. I.; De La Mata, M. Mid-Infrared Light-Emitting Diodes. In *Mid-Infrared Optoelectronics*; Tournié, E., Cerutti, L., Eds.; Elsevier, 2020; pp 59−90, DOI: 10.1016/B978-0-08-102709-7.00002-4.
(3) Popa, D.; Udrea, F. Towards Integrated Mid-Infrared Gas Sensors. *Sensors* **2019**, *19* (9), 2076.
(4) Hildenbrand, J.; Peter, C.; Lamprecht, F.; Kürzinger, A.; Naumann, F.; Ebert, M.; Wehrspohn, R.; Korvink, J. G.; Wöllenstein, J. Fast Transient Temperature Operating Micromachined Emitter for Mid-Infrared Optical Gas Sensing Systems: Design, Fabrication, Characterization and Optimization. *Microsyst. Technol.* **2010**, *16*, 745−754.
(5) Hodgkinson, J.; Tatam, R. P. Optical Gas Sensing: A Review. *Meas. Sci. Technol.* **2013**, *24* (1), 012004.
(6) Li, W.; Fan, S. Nanophotonic Control of Thermal Radiation for Energy Applications [Invited]. *Opt. Express* **2018**, *26* (12), 15995−16021.
(7) Baranov, D. G.; Xiao, Y.; Nechepurenko, I. A.; Krasnok, A.; Alù, A.; Kats, M. A. Nanophotonic Engineering of Far-Field Thermal Emitters. *Nat. Mater.* **2019**, *18* (9), 920−930.
(8) Wei, J.; Ren, Z.; Lee, C. Metamaterial Technologies for Miniaturized Infrared Spectroscopy: Light Sources, Sensors, Filters, Detectors, and Integration. *J. Appl. Phys.* **2020**, *128* (24), 240901.
(9) Greffet, J.-J.; Carminati, R.; Joulain, K.; Mulet, J.-P.; Mainguy, S.; Chen, Y. Coherent Emission of Light by Thermal Sources. *Nature* **2002**, *416* (6876), 61−64.
(10) Puscasu, I.; Schaich, W. L. Narrow-Band, Tunable Infrared Emission from Arrays of Microstrip Patches. *Appl. Phys. Lett.* **2008**, *92*, 233102.
(11) Schuller, J. A.; Taubner, T.; Brongersma, M. L. Optical Antenna Thermal Emitters. *Nature Photon* **2009**, *3* (11), 658−661.
(12) Liu, X.; Tyler, T.; Starr, T.; Starr, A. F.; Jokerst, N. M.; Padilla, W. J. Taming the Blackbody with Infrared Metamaterials as Selective Thermal Emitters. *Phys. Rev. Lett.* **2011**, *107* (4), 045901.
(13) Inoue, T.; De Zoysa, M.; Asano, T.; Noda, S. Realization of Narrowband Thermal Emission with Optical Nanostructures. *Optica* **2015**, *2* (1), 27−35.
(14) Wang, T.; Li, P.; Chigrin, D. N.; Giles, A. J.; Bezares, F. J.; Glembocki, O. J.; Caldwell, J. D.; Taubner, T. Phonon-Polaritonic Bowtie Nanoantennas: Controlling Infrared Thermal Radiation at the Nanoscale. *ACS Photonics* **2017**, *4* (7), 1753−1760.
(15) Shin, S.; Elzouka, M.; Prasher, R.; Chen, R. Far-Field Coherent Thermal Emission from Polaritonic Resonance in Individual Anisotropic Nanoribbons. *Nat. Commun.* **2019**, *10* (1), 1377.
(16) Kudyshev, Z. A.; Kildishev, A. V.; Shalaev, V. M.; Boltasseva, A. Machine-Learning-Assisted Metasurface Design for High-Efficiency Thermal Emitter Optimization. *Appl. Phys. Rev.* **2020**, *7* (2), 021407.
(17) Suemitsu, M.; Asano, T.; Inoue, T.; Noda, S. High-Efficiency Thermophotovoltaic System That Employs an Emitter Based on a Silicon Rod-Type Photonic Crystal. *ACS Photonics* **2020**, *7* (1), 80−87.
(18) He, M.; Nolen, J. R.; Nordlander, J.; Cleri, A.; McIlwaine, N. S.; Tang, Y.; Lu, G.; Folland, T. G.; Landman, B. A.; Maria, J.-P.; Caldwell, J. D. Deterministic Inverse Design of Tamm Plasmon Thermal Emitters with Multi-Resonant Control. *Nat. Mater.* **2021**, *20* (12), 1663−1669.
(19) Overvig, A. C.; Mann, S. A.; Alù, A. Thermal Metasurfaces: Complete Emission Control by Combining Local and Nonlocal Light-Matter Interactions. *Phys. Rev. X* **2021**, *11* (2), 021050.
(20) Zhao, B.; Song, J.-H.; Brongersma, M.; Fan, S. Atomic-Scale Control of Coherent Thermal Radiation. *ACS Photonics* **2021**, *8* (3), 872−878.
(21) Zhou, M.; Khoram, E.; Liu, D.; Liu, B.; Fan, S.; Povinelli, M. L.; Yu, Z. Self-Focused Thermal Emission and Holography Realized by Mesoscopic Thermal Emitters. *ACS Photonics* **2021**, *8* (2), 497−504.
(22) Inoue, T.; Zoysa, M. D.; Asano, T.; Noda, S. Realization of Dynamic Thermal Emission Control. *Nat. Mater.* **2014**, *13* (10), 928−931.
(23) Brar, V. W.; Sherrott, M. C.; Jang, M. S.; Kim, S.; Kim, L.; Choi, M.; Sweatlock, L. A.; Atwater, H. A. Electronic Modulation of Infrared Radiation in Graphene Plasmonic Resonators. *Nat. Commun.* **2015**, *6* (1), 7032.
(24) Xiao, Y.; Charipar, N. A.; Salman, J.; Piqué, A.; Kats, M. A. Nanosecond Mid-Infrared Pulse Generation via Modulated Thermal Emissivity. *Light Sci. Appl.* **2019**, *8*, 51.
(25) Song, B.; Liu, F.; Wang, H.; Miao, J.; Chen, Y.; Kumar, P.; Zhang, H.; Liu, X.; Gu, H.; Stach, E. A.; Liang, X.; Liu, S.; Fakhraai, Z.; Jariwala, D. Giant Gate-Tunability of Complex Refractive Index in Semiconducting Carbon Nanotubes. *ACS Photonics* **2020**, *7* (10), 2896−2905.
(26) Zou, Y.; Pan, H.; Huang, S.; Chen, P.; Yan, H.; An, Z. Non-Planckian Infrared Emission from GaAs Devices with Electrons and Lattice out-of-Thermal-Equilibrium. *Opt. Express* **2021**, *29* (2), 1244−1250.
(27) Pyatkov, F.; Fütterling, V.; Khasminskaya, S.; Flavel, B. S.; Hennrich, F.; Kappes, M. M.; Krupke, R.; Pernice, W. H. P. Cavity-Enhanced Light Emission from Electrically Driven Carbon Nanotubes. *Nat. Photonics* **2016**, *10* (6), 420−427.
(28) Miyoshi, Y.; Fukazawa, Y.; Amasaka, Y.; Reckmann, R.; Yokoi, T.; Ishida, K.; Kawahara, K.; Ago, H.; Maki, H. High-Speed and on-Chip Graphene Blackbody Emitters for Optical Communications by Remote Heat Transfer. *Nat. Commun.* **2018**, *9* (1), 1279.
(29) Shi, C.; Mahlmeister, N. H.; Luxmoore, I. J.; Nash, G. R. Metamaterial-Based Graphene Thermal Emitter. *Nano Res.* **2018**, *11*, 3567−3573.
(30) Kim, Y. D.; Gao, Y.; Shiue, R.-J.; Wang, L.; Aslan, O. B.; Bae, M.-H.; Kim, H.; Seo, D.; Choi, H.-J.; Kim, S. H.; Nemilentsau, A.; Low, T.; Tan, C.; Efetov, D. K.; Taniguchi, T.; Watanabe, K.; Shepard, K. L.; Heinz, T. F.; Englund, D.; Hone, J. Ultrafast Graphene Light Emitters. *Nano Lett.* **2018**, *18* (2), 934−940.
(31) Brouillet, J.; Papadakis, G. T.; Atwater, H. A. Experimental Demonstration of Tunable Graphene-Polaritonic Hyperbolic Metamaterial. *Opt. Express* **2019**, *27* (21), 30225−30232.
(32) Kocer, H.; Cakir, M. C.; Durna, Y.; Soydan, M. C.; Odabasi, O.; Isik, H.; Aydın, K.; Özbay, E. Exceptional Adaptable MWIR Thermal

Emission for Ordinary Objects Covered with Thin VO_2 Film. *J. Quant. Spectrosc. Radiat. Transfer* **2021**, *262*, 107500.
(33) Mori, T.; Yamauchi, Y.; Honda, S.; Maki, H. An Electrically Driven, Ultrahigh-Speed, on-Chip Light Emitter Based on Carbon Nanotubes. *Nano Lett.* **2014**, *14* (6), 3277−3283.
(34) Sakat, E.; Wojszvzyk, L.; Hugonin, J.-P.; Besbes, M.; Sauvan, C.; Greffet, J.-J. Enhancing Thermal Radiation with Nanoantennas to Create Infrared Sources with High Modulation Rates. *Optica* **2018**, *5* (2), 175−179.
(35) Wojszvzyk, L.; Nguyen, A.; Coutrot, A.-L.; Zhang, C.; Vest, B.; Greffet, J.-J. An Incandescent Metasurface for Quasimonochromatic Polarized Mid-Wave Infrared Emission Modulated beyond 10 MHz. *Nat. Commun.* **2021**, *12*, 1492.
(36) Fujiwara, M.; Tsuya, D.; Maki, H. Electrically Driven, Narrow-Linewidth Blackbody Emission from Carbon Nanotube Microcavity Devices. *Appl. Phys. Lett.* **2013**, *103* (14), 143122.
(37) He, X.; Gao, W.; Xie, L.; Li, B.; Zhang, Q.; Lei, S.; Robinson, J. M.; Hároz, E. H.; Doorn, S. K.; Wang, W.; Vajtai, R.; Ajayan, P. M.; Adams, W. W.; Hauge, R. H.; Kono, J. Wafer-Scale Monodomain Films of Spontaneously Aligned Single-Walled Carbon Nanotubes. *Nat. Nanotechnol.* **2016**, *11* (7), 633−638.
(38) Gao, W.; Komatsu, N.; Taylor, L. W.; Naik, G. V.; Yanagi, K.; Pasquali, M.; Kono, J. Macroscopically Aligned Carbon Nanotubes for Flexible and High-Temperature Electronics, Optoelectronics, and Thermoelectrics. *J. Phys. D: Appl. Phys.* **2020**, *53* (6), 063001.
(39) Tulevski, G. S.; Falk, A. L. Emergent Properties of Macroscale Assemblies of Carbon Nanotubes. *Adv. Funct. Mater.* **2020**, *30*, 1909448.
(40) Roberts, J. A.; Yu, S.-J.; Ho, P.-H.; Schoeche, S.; Falk, A. L.; Fan, J. A. Tunable Hyperbolic Metamaterials Based on Self-Assembled Carbon Nanotubes. *Nano Lett.* **2019**, *19* (5), 3131−3137.
(41) Schöche, S.; Ho, P.-H.; Roberts, J. A.; Yu, S. J.; Fan, J. A.; Falk, A. L. Mid-IR and UV-Vis-NIR Mueller Matrix Ellipsometry Characterization of Tunable Hyperbolic Metamaterials Based on Self-Assembled Carbon Nanotubes. *J. Vac. Sci. Technol. B* **2020**, *38* (1), 014015.
(42) Bondarev, I. V.; Adhikari, C. M. Collective Excitations and Optical Response of Ultrathin Carbon-Nanotube Films. *Phys. Rev. Applied* **2021**, *15* (3), 034001.
(43) Adhikari, C. M.; Bondarev, I. V. Controlled Exciton−Plasmon Coupling in a Mixture of Ultrathin Periodically Aligned Single-Wall Carbon Nanotube Arrays. *J. Appl. Phys.* **2021**, *129*, 015301.
(44) Roberts, J. A.; Ho, P.-H.; Yu, S.-J.; Wu, X.; Luo, Y.; Wilson, W. L.; Falk, A. L.; Fan, J. A. Multiple Tunable Hyperbolic Resonances in Broadband Infrared Carbon-Nanotube Metamaterials. *Phys. Rev. Applied* **2020**, *14* (4), 044006.
(45) Gao, W.; Doiron, C. F.; Li, X.; Kono, J.; Naik, G. V. Macroscopically Aligned Carbon Nanotubes as a Refractory Platform for Hyperbolic Thermal Emitters. *ACS Photonics* **2019**, *6* (7), 1602−1609.
(46) Sveningsson, M.; Jönsson, M.; Nerushev, O. A.; Rohmund, F.; Campbell, E. E. B. Blackbody Radiation from Resistively Heated Multiwalled Carbon Nanotubes during Field Emission. *Appl. Phys. Lett.* **2002**, *81* (6), 1095−1097.
(47) Li, P.; Jiang, K.; Liu, M.; Li, Q.; Fan, S.; Sun, J. Polarized Incandescent Light Emission from Carbon Nanotubes. *Appl. Phys. Lett.* **2003**, *82* (11), 1763−1765.
(48) Mann, D.; Kato, Y. K.; Kinkhabwala, A.; Pop, E.; Cao, J.; Wang, X.; Zhang, L.; Wang, Q.; Guo, J.; Dai, H. Electrically Driven Thermal Light Emission from Individual Single-Walled Carbon Nanotubes. *Nat. Nanotechnol.* **2007**, *2*, 33−38.
(49) Liu, P.; Liu, L.; Wei, Y.; Liu, K.; Chen, Z.; Jiang, K.; Li, Q.; Fan, S. Fast High-Temperature Response of Carbon Nanotube Film and Its Application as an Incandescent Display. *Adv. Mater.* **2009**, *21*, 3563−3566.
(50) Liu, Z.; Bushmaker, A.; Aykol, M.; Cronin, S. B. Thermal Emission Spectra from Individual Suspended Carbon Nanotubes. *ACS Nano* **2011**, *5* (6), 4634−4640.
(51) Bao, W.; Pickel, A. D.; Zhang, Q.; Chen, Y.; Yao, Y.; Wan, J.; Fu, K.; Wang, Y.; Dai, J.; Zhu, H.; Drew, D.; Fuhrer, M.; Dames, C.; Hu, L. Flexible, High Temperature, Planar Lighting with Large Scale Printable Nanocarbon Paper. *Adv. Mater.* **2016**, *28*, 4684−4691.
(52) Matano, S.; Takahashi, H.; Komatsu, N.; Shimura, Y.; Nakagawa, K.; Kono, J.; Maki, H. Electrical Generation of Polarized Broadband Radiation from an On-Chip Aligned Carbon Nanotube Film. *ACS Materials Lett.* **2022**, *4*, 626−633.
(53) Yudasaka, M.; Kataura, H.; Ichihashi, T.; Qin, L.-C.; Kar, S.; Iijima, S. Diameter Enlargement of HipCo Single-Wall Carbon Nanotubes by Heat Treatment. *Nano Lett.* **2001**, *1* (9), 487−489.
(54) Yang, X.; Yao, J.; Rho, J.; Yin, X.; Zhang, X. Experimental Realization of Three-Dimensional Indefinite Cavities at the Nanoscale with Anomalous Scaling Laws. *Nat. Photonics* **2012**, *6* (7), 450−454.
(55) Feng, K.; Harden, G.; Sivco, D. L.; Hoffman, A. J. Subdiffraction Confinement in All-Semiconductor Hyperbolic Metamaterial Resonators. *ACS Photonics* **2017**, *4* (7), 1621−1626.
(56) Sun, J.; Litchinitser, N. M.; Zhou, J. Indefinite by Nature: From Ultraviolet to Terahertz. *ACS Photonics* **2014**, *1* (4), 293−303.
(57) Chang, Y.-C.; Liu, C.-H.; Liu, C.-H.; Zhang, S.; Marder, S. R.; Narimanov, E. E.; Zhong, Z.; Norris, T. B. Realization of Mid-Infrared Graphene Hyperbolic Metamaterials. *Nat. Commun.* **2016**, *7*, 10568.
(58) Chiu, K.-C.; Falk, A. L.; Ho, P.-H.; Farmer, D. B.; Tulevski, G.; Lee, Y.-H.; Avouris, P.; Han, S.-J. Strong and Broadly Tunable Plasmon Resonances in Thick Films of Aligned Carbon Nanotubes. *Nano Lett.* **2017**, *17* (9), 5641−5645.
(59) Ho, P.-H.; Farmer, D. B.; Tulevski, G. S.; Han, S.-J.; Bishop, D. M.; Gignac, L. M.; Bucchignano, J.; Avouris, P.; Falk, A. L. Intrinsically Ultrastrong Plasmon−Exciton Interactions in Crystallized Films of Carbon Nanotubes. *Proc. Natl. Acad. Sci. U.S.A.* **2018**, *115* (50), 12662−12667.
(60) Griffiths, P. R.; De Haseth, J. A. *Fourier Transform Infrared Spectrometry*, 2nd ed.; John Wiley & Sons, Inc.: Hoboken, NJ, 2007.
(61) Xiao, Y.; Shahsafi, A.; Wan, C.; Roney, P. J.; Joe, G.; Yu, Z.; Salman, J.; Kats, M. A. Measuring Thermal Emission near Room Temperature Using Fourier-Transform Infrared Spectroscopy. *Phys. Rev. Applied* **2019**, *11* (1), 014026.
(62) Xiao, Y.; Wan, C.; Shahsafi, A.; Salman, J.; Yu, Z.; Wambold, R.; Mei, H.; Perez, B. E. R.; Derdeyn, W.; Yao, C.; Kats, M. A. Precision Measurements of Temperature-Dependent and Non-equilibrium Thermal Emitters. *Laser Photonics Rev.* **2020**, *14* (8), 1900443.
(63) Falk, A. L.; Chiu, K.-C.; Farmer, D. B.; Cao, Q.; Tersoff, J.; Lee, Y.-H.; Avouris, P.; Han, S.-J. Coherent Plasmon and Phonon-Plasmon Resonances in Carbon Nanotubes. *Phys. Rev. Lett.* **2017**, *118* (25), 257401.
(64) Greffet, J.-J.; Bouchon, P.; Brucoli, G.; Marquier, F. Light Emission by Nonequilibrium Bodies: Local Kirchhoff Law. *Phys. Rev. X* **2018**, *8* (2), 021008.
(65) Yamaguchi, S.; Tsunekawa, I.; Komatsu, N.; Gao, W.; Shiga, T.; Kodama, T.; Kono, J.; Shiomi, J. One-Directional Thermal Transport in Densely Aligned Single-Wall Carbon Nanotube Films. *Appl. Phys. Lett.* **2019**, *115* (22), 223104.
(66) Behabtu, N.; Young, C. C.; Tsentalovich, D. E.; Kleinerman, O.; Wang, X.; Ma, A. W. K.; Bengio, E. A.; ter Waarbeek, R. F.; de Jong, J. J.; Hoogerwerf, R. E.; Fairchild, S. B.; Ferguson, J. B.; Maruyama, B.; Kono, J.; Talmon, Y.; Cohen, Y.; Otto, M. J.; Pasquali, M. Strong, Light, Multifunctional Fibers of Carbon Nanotubes with Ultrahigh Conductivity. *Science* **2013**, *339* (6116), 182−186.
(67) Hone, J.; Llaguno, M. C.; Biercuk, M. J.; Johnson, A. T.; Batlogg, B.; Benes, Z.; Fischer, J. E. Thermal Properties of Carbon Nanotubes and Nanotube-Based Materials. *Appl. Phys. A: Mater. Sci. Process.* **2002**, *74*, 339−343.
(68) Lochbaum, A.; Dorodnyy, A.; Koch, U.; Koepfli, S. M.; Volk, S.; Fedoryshyn, Y.; Wood, V.; Leuthold, J. Compact Mid-Infrared Gas Sensing Enabled by an All-Metamaterial Design. *Nano Lett.* **2020**, *20* (6), 4169−4176.
(69) Livingood, A.; Nolen, J. R.; Folland, T. G.; Potechin, L.; Lu, G.; Criswell, S.; Maria, J.-P.; Shelton, C. T.; Sachet, E.; Caldwell, J. D.

https://doi.org/10.1021/acs.nanolett.2c01579
Nano Lett. 2022, 22, 5832−5840

Filterless Nondispersive Infrared Sensing Using Narrowband Infrared Emitting Metamaterials. *ACS Photonics* **2021**, *8* (2), 472−480.
(70) Pusch, A.; De Luca, A.; Oh, S. S.; Wuestner, S.; Roschuk, T.; Chen, Y.; Boual, S.; Ali, Z.; Phillips, C. C.; Hong, M.; Maier, S. A.; Udrea, F.; Hopper, R. H.; Hess, O. A Highly Efficient CMOS Nanoplasmonic Crystal Enhanced Slow-Wave Thermal Emitter Improves Infrared Gas-Sensing Devices. *Sci. Rep.* **2015**, *5* (1), 17451.
(71) Hasan, D.; Lee, C. Hybrid Metamaterial Absorber Platform for Sensing of CO_2 Gas at Mid-IR. *Adv. Sci.* **2018**, *5* (5), 1700581.
(72) Walker, J. S.; Fagan, J. A.; Biacchi, A. J.; Kuehl, V. A.; Searles, T. A.; Hight Walker, A. R.; Rice, W. D. Global Alignment of Solution-Based Single-Wall Carbon Nanotube Films via Machine-Vision Controlled Filtration. *Nano Lett.* **2019**, *19* (10), 7256−7264.
(73) Ma, W.; Alonso-González, P.; Li, S.; Nikitin, A. Y.; Yuan, J.; Martín-Sánchez, J.; Taboada-Gutiérrez, J.; Amenabar, I.; Li, P.; Vélez, S.; Tollan, C.; Dai, Z.; Zhang, Y.; Sriram, S.; Kalantar-Zadeh, K.; Lee, S.-T.; Hillenbrand, R.; Bao, Q. In-Plane Anisotropic and Ultra-Low-Loss Polaritons in a Natural van Der Waals Crystal. *Nature* **2018**, *562*, 557−562.
(74) Wang, C.; Huang, S.; Xing, Q.; Xie, Y.; Song, C.; Wang, F.; Yan, H. Van Der Waals Thin Films of WTe 2 for Natural Hyperbolic Plasmonic Surfaces. *Nat. Commun.* **2020**, *11* (1), 1158.
(75) Wang, F.; Wang, C.; Chaves, A.; Song, C.; Zhang, G.; Huang, S.; Lei, Y.; Xing, Q.; Mu, L.; Xie, Y.; Yan, H. Prediction of Hyperbolic Exciton-Polaritons in Monolayer Black Phosphorus. *Nat. Commun.* **2021**, *12* (1), 5628.
(76) Yu, S.-J.; Jiang, Y.; Roberts, J. A.; Huber, M. A.; Yao, H.; Shi, X.; Bechtel, H. A.; Gilbert Corder, S. N.; Heinz, T. F.; Zheng, X.; Fan, J. A. Ultrahigh-Quality Infrared Polaritonic Resonators Based on Bottom-Up-Synthesized van Der Waals Nanoribbons. *ACS Nano* **2022**, *16* (2), 3027−3035.

https://doi.org/10.1021/acs.nanolett.2c01579
Nano Lett. 2022, 22, 5832−5840